RESEARCH ARTICLE | FEBRUARY 13 2025

Anisotropic Ta₂O₅ photonic crystal waveguide etching using inductively coupled plasma etching

Wenjie Wang **■** ⑤ ; Libe Arzubiaga; Maryam Shayesteh; Stephen Fenner ⑥ ; Owain Clark; Martin D. B. Charlton ⑥



J. Vac. Sci. Technol. A 43, 023405 (2025) https://doi.org/10.1116/6.0004211





Articles You May Be Interested In

Anisotropic ${\rm Ta_2O_5}$ waveguide etching using inductively coupled plasma etching

J. Vac. Sci. Technol. A (June 2014)

SiC via fabrication for wide-band-gap high electron mobility transistor/microwave monolithic integrated circuit devices

J. Vac. Sci. Technol. B (March 2008)

Smooth reactive ion etching of GaAs using a hydrogen plasma pretreatment

J. Vac. Sci. Technol. B (January 1995)





Anisotropic Ta₂O₅ photonic crystal waveguide etching using inductively coupled plasma etching

Cite as: J. Vac. Sci. Technol. A 43, 023405 (2025); doi: 10.1116/6.0004211 Submitted: 15 November 2024 · Accepted: 29 January 2025 · Published Online: 13 February 2025







Wenjie Wang,^{1,a)} 📵 Libe Arzubiaga,² Maryam Shayesteh, ¹ Stephen Fenner, ¹ 📵 Owain Clark, ² and Martin D. B. Charlton 1 00

AFFILIATIONS

- ¹School of Electronics and Computer Science, University of Southampton, Southampton SO17 1BJ, United Kingdom ²Southampton Nanofabrication Centre, Optoelectronics Research Centre, University of Southampton, Southampton SO17 1BJ, United Kingdom
- a) Author to whom correspondence should be addressed: ww2m19@soton.ac.uk

ABSTRACT

Achieving smooth and vertical sidewall profile in the 2D photonic crystals (PhCs) is crucial for the photonic crystal waveguides (PCWs) in integrated optical devices, since "volcano" shaped PhCs lead to light leakage and the drift of photonic bandgap. This paper optimizes the inductively coupled plasma reactive ion etching (ICP-RIE) process for improving the sidewall profile of Ta₂O₅ PCW with minimum PhC dimension of 300 nm pitch and 185 nm diameter. A set of experiments was generated by statistical software (MINITAB) to efficiently investigate the region of interest in the process space by varying RF platen power, ICP power, $%C_4F_8$ in gas mixture (C_4F_8 and O_2), and chamber pressure. Subsequently, the most suitable experimental conditions were identified and used as the central run for analyzing the influence of S individual parameters on ICP etching of Ta₂O₅. Key findings include the importance of maintaining a 50% C₄F₈ in total gas flow and trade-offs related to ICP and RF power adjustments. Pressure has a negligible impact on sidewall angle but exerts a more pronounced influence on etch rate and micromasking. A delicate balance among these parameters is crucial for optimal etching results. The recommended recipe (50 W RF platen power, 2000 W ICP power, 10 mTorr pressure, 50% C₄F₈ in total gas flow) achieves an etch rate of 113.325 nm/min with a smooth and vertical sidewall in PhCs. The entire etching exploration process was conducted on a Ta2O5 layer deposited on a Si substrate. Additionally, this recipe was applied to etch Ta₂O₅ with a 2 µm SiO₂ layer interposed between the Ta₂O₅ layer and the Si substrate, yielding favorable results and preserving the integrity of the PhC sidewall.

© 2025 Author(s). All article content, except where otherwise noted, is licensed under a Creative Commons Attribution (CC BY) license (https://creativecommons.org/licenses/by/4.0/). https://doi.org/10.1116/6.0004211

I. INTRODUCTION

Tantalum pentoxide (Ta₂O₅) is a promising material in optics and silicon photonics, since it has a high refractive index and its optical constants have been determined over a broad spectral region, from visible to the far infrared. Ta2O5 used in waveguides shows great potential for ultra-low loss C-band light guiding,2 higher-order mode supercontinuum generation,³ optical micropropulsion,⁴ on-chip amplifiers,5 and filters.6 Photonic crystals (PhCs) are periodic nanostructures, which are used to affect light propagation, and they create photonic bandgaps (PBGs), where no light within PBG frequency can propagate. Integrating PhC into silicon photonics would help to minimize the optical components, improve the lightmatter interaction, 9,10 and enhance nonlinear optical effects. 1

Photonic crystal waveguides (PCWs) are the fundamental components in the integration of PhCs into silicon photonics.

Inductively coupled plasma reactive ion etching (ICP-RIE) is one of the common methods used in Ta₂O₅ dry etching. Figure 1 presents a schematic diagram of an ICP etcher. Two RF generators play essential roles in plasma generation: the RIE RF generator and the cylindrical ICP RF generator. 12,13 The RIE RF generator creates plasma capacitively by RF excitation of parallel plate electrodes, ionizing the gas in the chamber and producing an electromagnetic field between the electrodes. The negative self-bias potential developed in between the parallel plates accelerates positive ions toward the sample, sitting onto the powered electrode. The ion energy can reach several hundred electron volts (eV), resulting in plasmas with



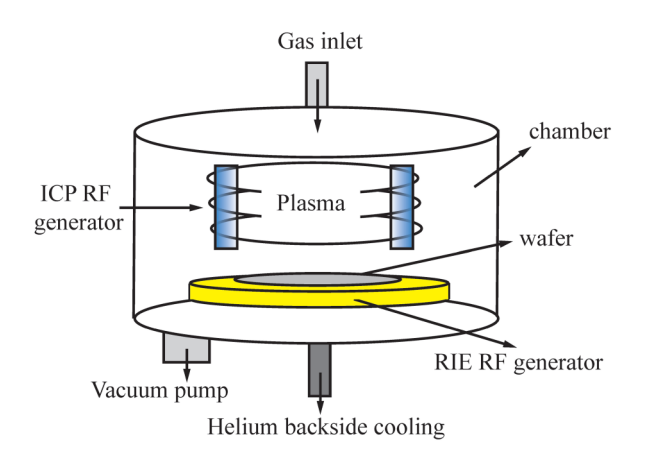


FIG. 1. Schematic diagram of the ICP etcher.

relatively high ion energy but low density. In contrast, the cylindrical ICP RF generator produces high-density inductively coupled plasma through RF excitation of a coil positioned outside the chamber and which is shielded to prevent any capacitive coupling. This coil generates an electromagnetic field within the chamber, which also ionizes the gas and creates a high-density plasma. The advantage of having both platen RIE and cylindrical ICP generators is that it offers the opportunity to separately tune the plasma density and the ion energy. Wafers are mechanically loaded, clamped, and helium-cooled on the backside to optimize thermal conductivity. The ICP process utilizes physical etching and chemical etching. Physical etching involves high-speed positive ion sputter etching; While in chemical etching, volatile products are produced as neutral reactive species generated by the plasma interacting with the material surface. 14,15 As for the etching characteristics, chemical etching provides high etch rates, high selectivity, and minimal ion bombardment-induced damage but yields isotropic profiles. In contrast, physical etching achieves anisotropic profiles with severe bombardment-induced damage and lower selectivity. 14 The combination of chemical and physical etching in ICP etcher yields anisotropic etch profiles with moderate damage.

Fluorine or chlorine-based chemistries were found to achieve maximum etch rates of around 120 nm/min for Ta₂O₅ ICP etching, compared with CH₄/H₂/Ar or N₂/Ar. ¹⁶ UV illumination during Ta₂O₅ ICP etching (using SF₆/Ar and Cl₂/Ar plasma chemistries) produces significant enhancements in etch rates due to the photoassisted desorption of TaCl_x and TaF_x etch products. The most recent paper related to Ta2O5 ICP etching is from Muttalib et al.,

TABLE I. ICP recipe suggested by Muttalib et al. (Ref. 18).

RF platen power (W)	ICP power (W)	C ₄ F ₈ /O ₂ gas flow (SCCM)	Chamber pressure (mTorr)
300	750	38/2	20

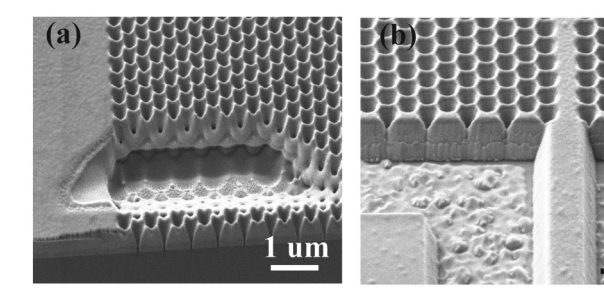


FIG. 2. (a) "Volcano"-shaped PhCs and (b) angled wire waveguide fabricated using the existing process recipe.

which thoroughly investigated the effect of key parameters (including ICP power, RF platen power, gas flow, and chamber pressure) on etch rate and sidewall slope angle, but it aims for wire waveguide. 18 There exists a study addressing the etching of Ta₂O₅ in the context of PhCs but utilizing the pulsed electron-cyclotron-resonance method.¹⁹ The other study involving the Ta₂O₅ PhC dry etching uses reactive ion etching (RIE) for narrow band grating-waveguide reflective filters, which use 50 nm intermediate Ge mask layer to make the sidewall smooth and vertical.6

The ICP recipe proposed by Muttalib et al., as shown in Table I, has drifted over the years due to equipment updates. Moreover, the current sample integrates PhCs, characterized by a minimum dimension featuring a pitch of 300 nm and a diameter of 185 nm. In contrast, the structure from Muttalib et al. comprises → wire waveguides with a minimum dimension of 600 nm width separated at approximately $200\,\mu\text{m}$ intervals. This necessitates the utiliarated at approximately $200\,\mu\text{m}$ intervals. This necessitates the utiliarated at approximately $200\,\mu\text{m}$ intervals. This necessitates the utiliarated at approximately $200\,\mu\text{m}$ intervals. zation of electron beam lithography (EBL). Due to EBL's higher patterning resolution in comparison to optical lithography, it enables the fabrication of smaller structures.¹³ In this work, the $\frac{14}{5}$ introduction of more intricate structure necessitates adjustments to the existing recipe to obtain optimum outcomes, as using the previous recipe resulted in "volcano" shaped PhCs and angled wire waveguides [see Figs. 2(a) and 2(b)]. Statistical software (MINITAB) was utilized to generate a set of nine experimental runs to evenly map the process space within the selected parameter range. This enabled us to identify a region with suitable conditions to obtain the desired results and provided the grounds for fine-tuning the etch process, adjusting one parameter at a time.

II. EXPERIMENT

Figure 3(a) presents the fabrication process flow for the testing wafer. A 450 nm Ta₂O₅ film was deposited on a 6 in. silicon wafer using a Helios ProXL (Leybold Optics) cathode sputtering system under vacuum condition. As a hard mask, a 75 nm thick Cr layer was then deposited using Lab700 (Leybold Optics) by electron beam evaporation. Following this, a uniform layer of approximately 400 nm ZEP520A and 60 nm Electra92 was applied by spin coating. The former is a typical positive resist for EBL, while the latter is used as a top coating to facilitate the dissipation of electrical charges during E-beam writing and reduce the associated image placement errors. After E-beam exposure, Electra92 was removed

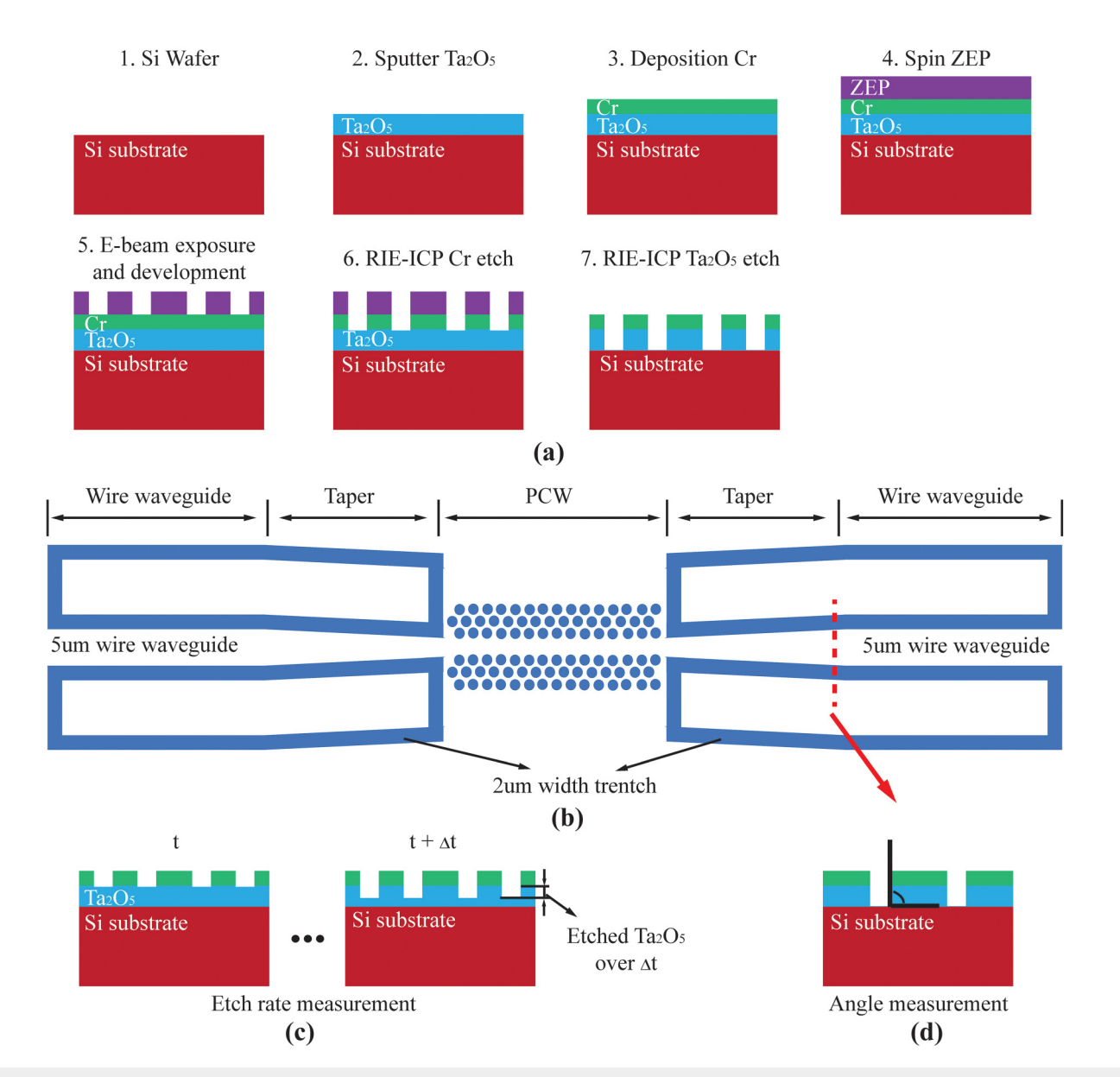


FIG. 3. (a) Fabrication process flow for the testing wafer of the PCW. (b) Schematic diagram of the PCW e-beam pattern, where colored regions represent exposed areas, and blank regions indicate unexposed, reserved areas. (c) Measurement of the Ta_2O_5 etch rate. (d) Angle measurement of the etched Ta_2O_5 layer.

by rinsing with water and the exposed resist layers were developed with ZED-N50. For the pattern transfer from ZEP520A to the Cr layer, Cl_2/O_2 (50/12.5 SCCM) based ICP etching was used, where the chamber pressure was set at 10 mTorr with ICP power at 750 W and RF platen power at 10 W. Both the Cr etching and the Ta_2O_5 etching were performed on a Plasmalab System 100 with a Cobra High Density Plasma (HDP) source of 380 mm from Oxford Instruments. The system operates with a 13.56 MHz capacitively coupled lower electrode, positioned below the wafer, as the RF platen generator, and a 2 MHz inductive coil as the ICP generator.

Based on the experience of Muttalib *et al.*, the fluorocarbon-based chemistry (C_4F_8 and O_2) was chosen to perform the Ta_2O_5 etching due to the possibility of benefiting from CF_x polymer-based sidewall protection for the control of the etch anisotropy.

Figure 3(b) illustrates the e-beam pattern used to test the Ta_2O_5 etch rate and sidewall angle. The PCW is created by removing a single row of PhCs. It is adiabatically tapered to a $5 \mu m$ wide wire waveguide, facilitating the coupling of light into and out of the PCWs. Both the taper and the wire waveguide are formed by etching $2 \mu m$ wide trenches on either side.

TABLE II. Lower, center, and upper settings for the initial set of experimental runs.

Parameter	Low setting	Center point	High setting
RF platen power (W)	50	100	150
ICP power (W)	1000	1500	2000
C_4F_8 in gas mixture $(C_4F_8$ and $O_2)$	40	67.5	95
Pressure (mTorr)	5	7.5	10

^aWhere the total gas flow is set to 100 SCCM, platen temperature is set to 20 °C, and the He backing pressure is set to 10 Torr.

The new recipe was developed at chip scale (approximate size $2\times 1.4\,\mathrm{cm}^2$) and then scaled up to full 6 in. wafer scale processing. The test chip incorporates different combinations of PhC characteristics, encompassing fill fractions of 0.35 and 0.45, with pitch values ranging from 300 to 390 nm in 30 nm step. To mimic a process wafer containing a majority surface area of Cr hard mask, test chips were mounted on a Cr-coated carrier wafer to prevent macroloading of the process with a large Si area. We used Santovac-5 vacuum oil as an interface material in between chips and carrier wafers for efficient thermal transfer and better control of temperature uniformity and stability.

Statistical software (MINITAB) was used to generate a total of nine combinations of the following parameters: RF platen power, ICP power, %C₄F₈ in gas mixture (C₄F₈, and O₂) and chamber pressure. Table II provides the boundaries selected for the studied parameters based on the available range within which our ICP tool can supply a stable plasma. Table III shows a summary of the nine experimental runs and the results obtained. To prepare the process chamber before the initial run, a 10 min O2-based plasma cleaning process followed by a 4 min conditioning step was performed. To ensure consistent conditions within the ICP chamber for every run, a short cleaning and conditioning routine was carried out—consisting of a fluorine-based plasma clean lasting twice the etch time of each run, followed by a 3 min O2-based plasma clean, and a subsequent 3 min conditioning process on a Cr-coated carrier wafer, using the same conditions of the corresponding run. For ease of measuring the angle and etch rate, the etched Ta₂O₅ is around 50%-70% of its total thickness. The sidewall angle is measured using the $2\mu m$ trench sidewall angle, since the region in PhCs is too tight to allow accurate measurement. Test chips were cleaved after etching and imaged with SEM to determine the etch rate and sidewall angles. Figures 3(c) and 3(d) provide schematic illustrations of the Ta2O5 etch rate and sidewall angle measurement methods, respectively.

III. RESULTS AND DISCUSSION

A. Initial etch experiment results

The nine different combinations of experiment parameters are listed in Table III. Repetitive runs (three repetitions of Run 2) yielded identical results, demonstrating consistency prior to conducting the full set of experiments. Figure 4 shows the cross-sectional SEM images for Runs 2, 4, 7, and 8, respectively.

Run 2 shows the best result where the PhC has a vertical sidewall
with less (nearly none) debris over the 2 μm trench. It has lower
RF platen power, higher ICP power, and a reasonable %C₄F₈ in

- total gas flow. It shows an excellent balance between physical and chemical etching.
- Run 4 shows the worst scenario of all nine runs. The RF platen power (and consequently, the ion bombardment energy) is low, which results in lower physical etching. Moreover, a higher %C₄F₈ in total gas flow promotes the formation of abundant CF_x polymer, which implies a lower chemical etching rate. This leads to a thin CF_x polymer layer formed and the PhCs being completely covered.
- Run 7 also has a higher C₄F₈ polymer ratio but with a higher RF platen power. A harsher physical etching cancels out the effect of having excessive polymerization originating from the fluorocarbon plasma, resulting in an angled PhC sidewall.
- Run 8 acts as an example showing moderate debris. These debris show up possibly due to higher RF platen power, since physical etching in ICP etching causes severe bombardment-induced damage, leading to uneven surfaces. Another assumption is that Cr debris are bombarded from the Cr layer and falls onto the Ta_2O_5 layer surface during the etching process, acting as a micromask for subsequent etching.

The small variation observed in the measured response (side- $\frac{36}{120}$) wall angle) did not allow to build a robust model to statistically predict optimum results and, therefore, no further analysis was done with MINITAB. The set of nine experiments was initially proposed to evenly sweep the region of interest in the process space and to identify suitable conditions to obtain the desired results in terms of etch rate and sidewall angle. This provided the grounds to further explore the impact of each parameter on the ICP-RIE process. By using the conditions in Run 2 as the center run, we, thus, varied one parameter at a time in order to study its individual effect in the Ta_2O_5 etch rate and sidewall angle. The results obtained are summarized in Subsections III B-III D.

B. RF platen and ICP power

Figure 5(a) shows the relationship between Ta_2O_5 etch rate and sidewall angle with respect to RF platen power. It can be observed that the etching rate increases with increasing RF platen power. This is due to the fact: it is RF platen power that supplies kinetic energy to the etchant ion species (that can be F_+ and CF_{x+}), which bombard the substrate. Increasing RF platen power leads to an increase in ion bombardment energy, which in turn leads to the rise of physical etching. The decrease in sidewall angle with increasing RF platen power is likely because of mask faceting, which happens due to the angular dependence of the sputtering (or physical etching) rate. Faceting

Run	RF platen power (W)	ICP power (W)	Pressure (mTorr)	$%C_4F_8$ in gas mixture $(C_4F_8 \text{ and } O_2)$	Etch rate (nm/min)	Angle (deg)	Micromasking
1	150	2000	5	50	98.2	73.5	None
2	50	2000	10	50	113.325	88.1	Few
3	100	1500	7.5	72.5	49.36	71.7	Severe
4	50	1000	10	95	**	**	* ^a
5	150	1000	5	95	61.7	71.7	Severe
6	50	2000	5	95	10.729	74.4	Severe
7	150	2000	10	95	85.675	70	Severe
8	150	1000	10	50	86.9	72.6	Moderate
9	50	1000	5	50	109.075	83.2	None

^aWhere * indicates measurement incapability in Run 4, as thick CF_x polymer was deposited on the chip surface, with no etching present.

mostly originates from the preferential sputtering (physical) etching for off-normal ions. It is an inherent problem to physical etches and could explain getting slopped profiles when the expected polymer redeposition is low. The angle of the facet gives a preferential plane for the subsequence etching process and the facet can, thus, propagate into the Ta2O5 layer. The cross-sectional SEM images in Figs. 5(b) and 5(c) illustrate the comparison of the PCWs with RF platen powers of 50 and 200 W, respectively.

TABLE III. Summary of Ta₂O₅ etch experiment conditions and results.

Figure 6(a) illustrates the relationship between Ta₂O₅ etch rate and sidewall angle with respect to the ICP power. Increasing the ICP power speeds up the etching rate and provides a more vertical sidewall. High-density inductively coupled plasma is generated by the cylindrical ICP RF generator. At a given pressure setting, high ICP power results in increased fragmentation of C₄F₈, leading to a higher concentration of ionized F+ species. Conversely, at low ICP power, a significant presence of ionized heavy molecules, such as CF_{x+} , is observed. The small mass of ionized F_+ species would be more easily to gain the kinetic energy from the 50 W RF platen power than heavy ionized molecules and being directed into the wafer surface. Abundance of reactive F+ species that results in chemical etching phenomenon dominating over the polymer redeposition, thus leading to high etch rate and high sidewall angle. The side effect of very high plasma density is the production of a rough etched surface. A comparison of ICP power levels at 1000, 2000, and 2500 W, as shown in Figs. 6(b), 6(d), and 6(f), clearly demonstrates an increase in micromasking effects. Meanwhile, Figs. 6(c), 6(e), and 6(g) present the PhC SEM images at the corresponding ICP power levels, revealing a noticeable improvement in the sidewall angle with increasing ICP power.

C. $%C_4F_8$ in gas mixture (C_4F_8 and O_2)

the Ta_2O_5 etch rate and sidewall angle in relation to C_4F_8 . Learly, Ta_2O_5 etch rate is inversely proportional to C_4F_8 . presence of more O₂ will accelerate the Ta₂O₅ etch rate.

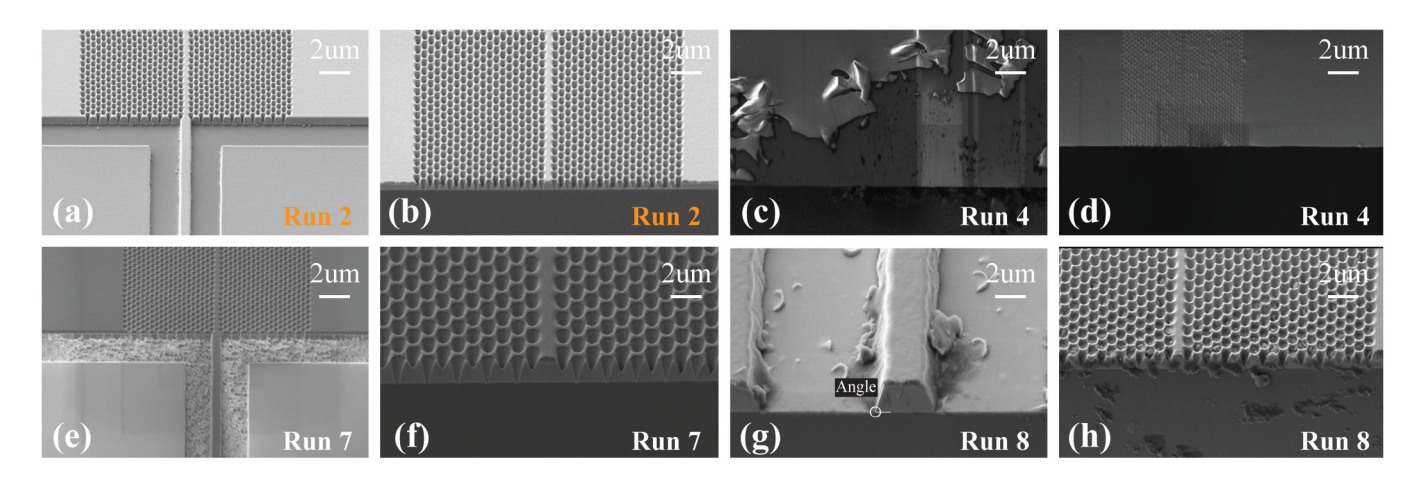
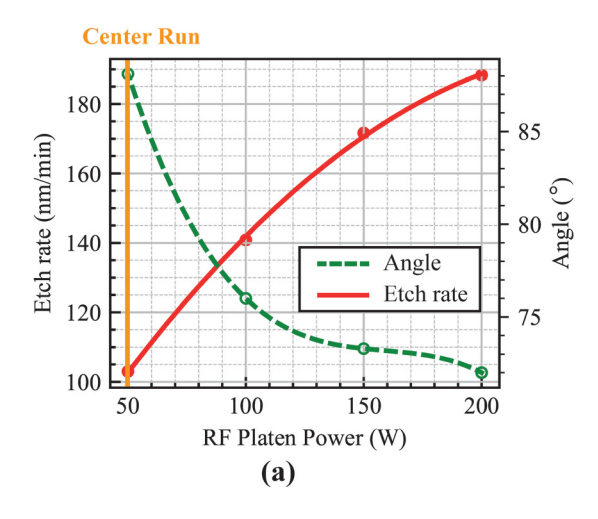


FIG. 4. SEM images with the PhCs dimension: pitch (390 nm) and diameter (245 nm). For Run 2: (a) junction of wire waveguide and PCW; (b) PhC image. For Run 4: (c) peeled polymer layer; (d) top-view SEM image of PhC. For Run 7: (e) junction of wire waveguide and PCW; (f) PhC image. For Run 8: (g) wire waveguide; (h) PhC



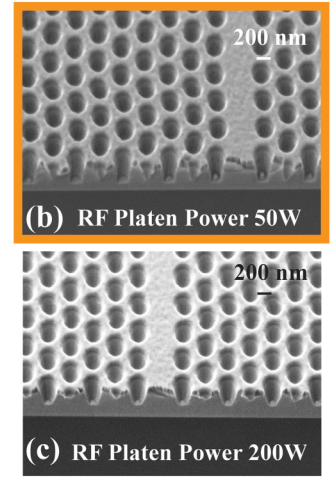
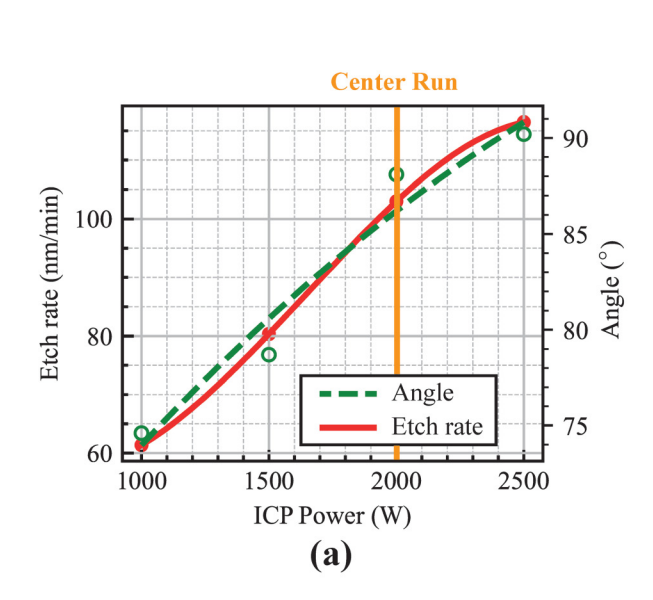


FIG. 5. (a) Effect of RF platen power on the ${\rm Ta_2O_5}$ etch rate and sidewall angle, with fixed parameters: 50% ${\rm C_4F_8}$ in total gas flow (100 SCCM), 2000 W ICP power, and 10 mTorr pressure. (b) PhC SEM image at 50 W RF platen power. (c) PhC SEM image at 200 W RF platen power.

A better understanding of this trend can be gained by exploring how C_4F_8 and O_2 function in chemical etching. In Ta_2O_5 etching, C_4F_8 performs multiple functions: On the one hand, it contains C for the formation of CF_x polymer-like species that provide sidewall

protection and enable an anisotropic etch. On the other hand, it provides F for the etching of Ta_2O_5 by forming volatile molecules TaF_4 . If the excess of CF_x polymer deposited on the surfaces is not removed by forming volatile species (such as CO, CO_2 , and COF_2), they will



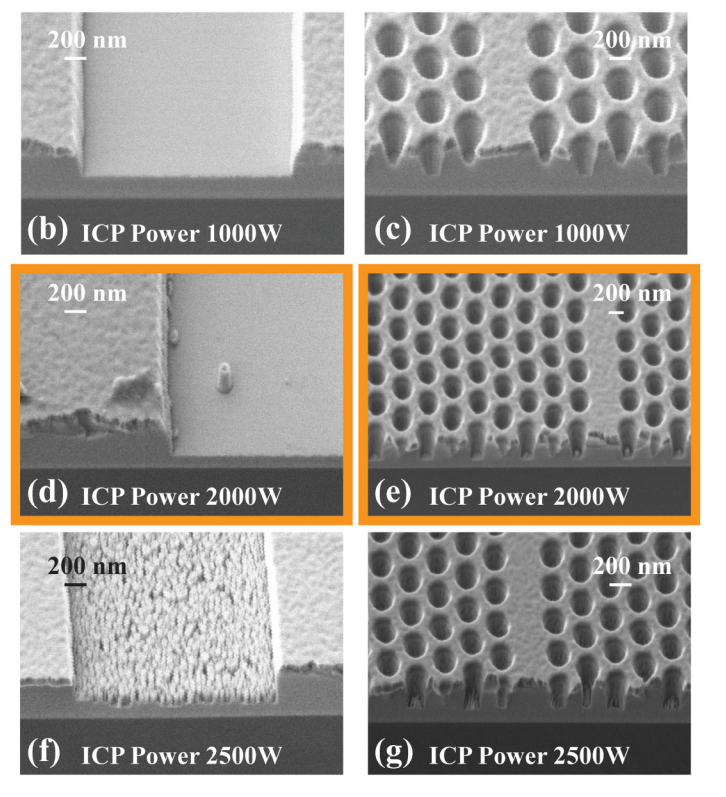


FIG. 6. (a) Effect of ICP power on the Ta₂O₅ etch rate and sidewall angle, with fixed parameters: 50% C₄F₈ in total gas flow (100 SCCM), 50 W RF platen power, and 10 mTorr pressure. (b) Trench and (c) PhC SEM images at 1000 W ICP power. (d) Trench and (e) PhC SEM images at 2000 W ICP power. (f) Trench and (g) PhC SEM images at 2500 W ICP power.

16 June 2025 11:16:41



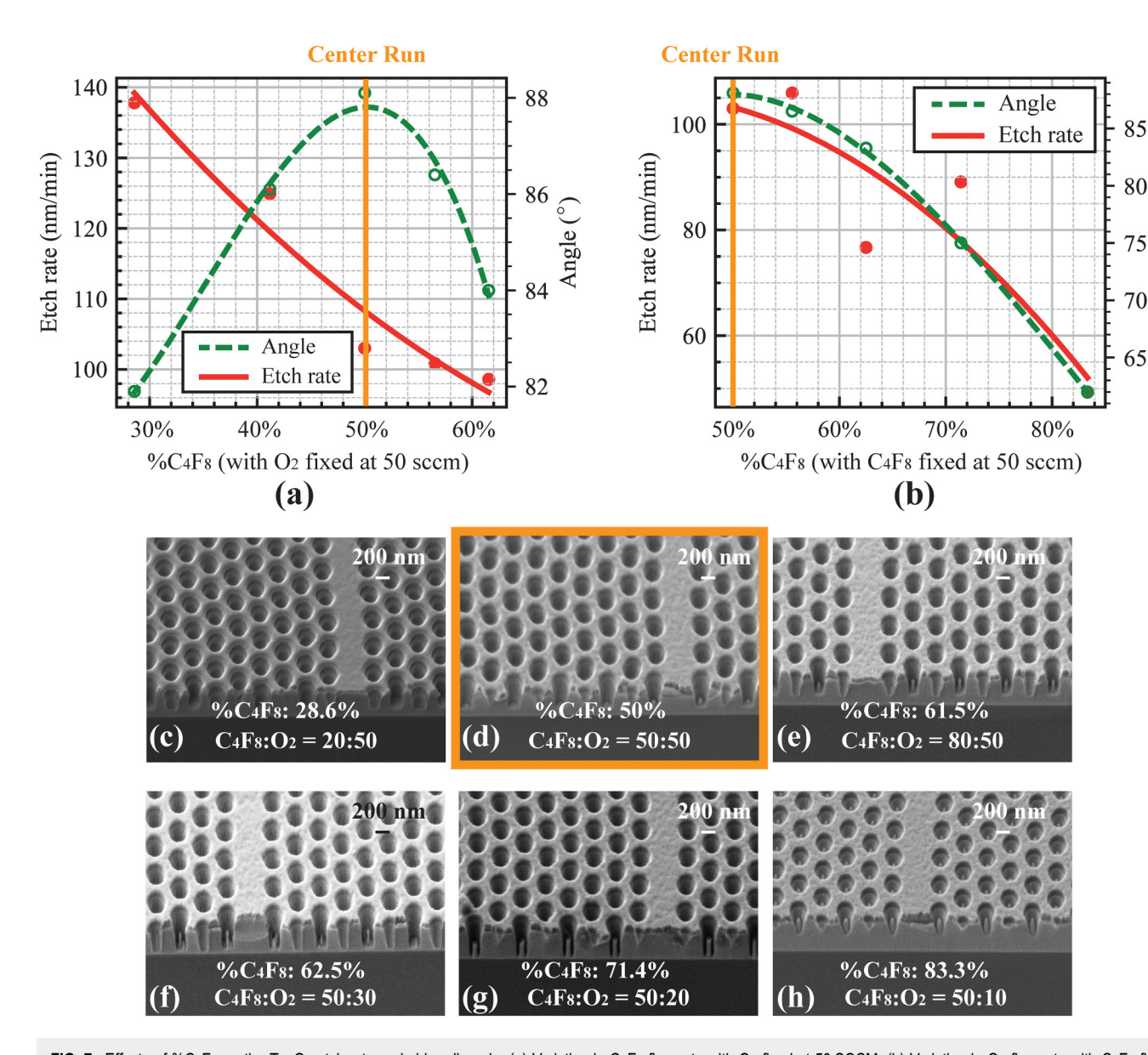
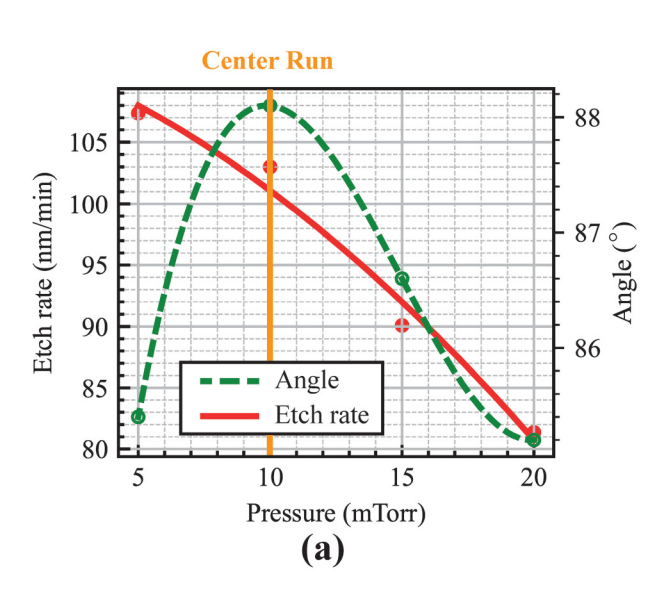


FIG. 7. Effects of %C₄F₈ on the Ta₂O₅ etch rate and sidewall angle. (a) Variation in C₄F₈ flow rate with O₂ fixed at 50 SCCM. (b) Variation in O₂ flow rate with C₄F₈ fixed at 50 SCCM. All other parameters are held constant: 10 mTorr chamber pressure, 50 W RF platen power, and 2000 W ICP power. (c)-(h) PhC SEM images with %C₄F₈ ranging from 28.6% to 83.3%.

become covered with a fluoropolymer film and etching will eventually stop. Oxygen can be sourced from either the O2 gas flow or it can evolve from the Ta₂O₅ etch itself. On the Cr surface, the only way to get rid of the carbon is to form volatile species such as CF₄. The CF_x polymer layer on the Ta₂O₅ is thinner than on the Cr surfaces, since the O evolved from the Ta₂O₅ etch promotes the formation of CO_x-like volatiles. A good compromise in between the polymer formation and depletion rate is crucial to obtain the desired sidewall angle in the etched features.

Figure 7(a) illustrates the effect of using different proportions of C_4F_8 gas flow (from 28% to 62%) on the sidewall angle of Ta_2O_5 . In the presence of too much C₄F₈, the polymerization function is boosted, resulting in more micromasking and a slower etching rate. In contrast, a lower level of C₄F₈ results in a clear etching surface but an isotropic etch for PhCs [see Fig. 7(c)], because sidewall protection is reduced and chemical reactions are enhanced. A good compromise is reached when C₄F₈ is 50% of the total gas flow. Figure 7(b) shows the transition from the optimum point (50% C₄F₈) until the excess



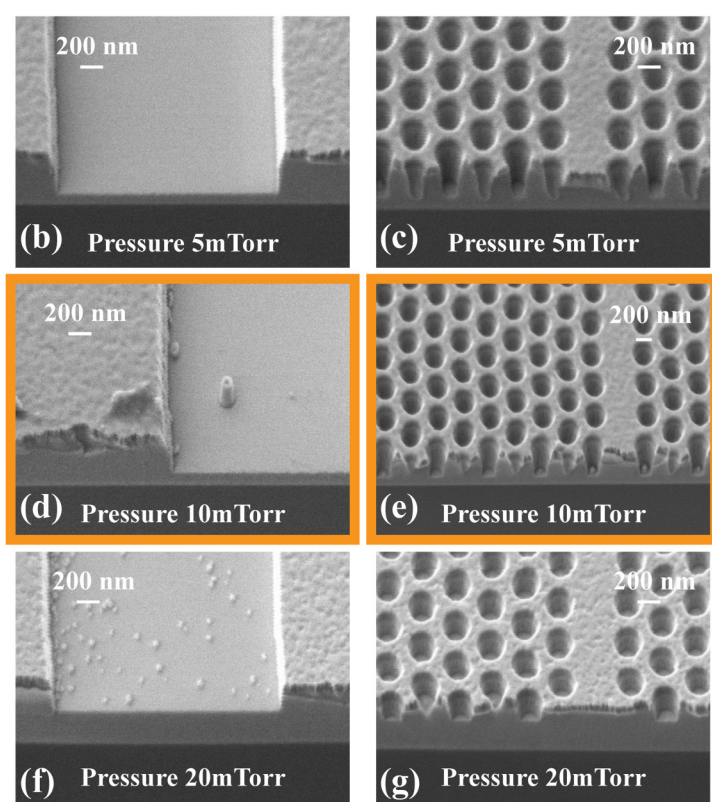


FIG. 8. (a) Effect of chamber pressure on the Ta_2O_5 etch rate and sidewall angle, with fixed process parameters: 50% C_4F_8 in total gas flow (100 SCCM), RF platen power of 50 W, and ICP power of 2000 W. (b) Trench and (c) PhC SEM images at 5 mTorr pressure. (d) Trench and (e) PhC SEM images at 10 mTorr pressure. (f) Trench and (g) PhC SEM images at 20 mTorr pressure.

polymerization at 83% C_4F_8 on Ta_2O_5 sidewall angle. When the C_4F_8 is over 50%, there are pillars inside the PhCs [see Figs. 7(e)–7(h)], which indicates that excess polymerization has overridden etching.

D. Chamber pressure

The Ta_2O_5 etch rate and sidewall angle in relation to chamber pressure is provided in Fig. 8(a). It is evident from the curve that Ta_2O_5 etch rate decreases with increasing pressure. Additionally, micromasking becomes more problematic at high pressures by observing 2 μ m trench status [see Figs. 8(b), 8(d), and 8(f)]. Pressure is believed to affect the rate of polymer deposition, and a higher pressure results in a faster deposition rate. Providing the total gas flow (100 SCCM) and C_4F_8 (50%) stays unchanged, as well as the RF platen (50 W) and ICP (2000 W) power, low level of the reactive F_+ species would be present in high pressure systems. This is due to the effect of a short mean free path, which is a contributing parameter to the fragmentation of precursor C_4F_8 molecule gas. Large amounts of CF_{x+} are present at higher pressure, which are responsible for redeposition (polymer formation), thus leading to lower etch rate, low sidewall angle, and more problematic debris.

Despite the fact that the best point for sidewall angle is found when the pressure is 10 mTorr, it is worth noting that all angles are

within 85°-88°, which is a relatively small change over pressure changes. Similarly, the SEM images of the PhCs did not change significantly as the pressure varies [see Figs. 8(c), 8(e), and 8(g)].

E. Ta_2O_5 etching with 2 μm SiO₂ layer placed beneath Ta_2O_5 layer

Although the etching process was optimized for a Ta₂O₅ layer on a Si substrate, this structure does not support light propagation. Light transmission occurs only in a sandwich structure with a low-high-low refractive index configuration, which enables light confinement and guiding through the principle of total internal reflection. Thus, the Ta₂O₅ etch experiment (using the recipe from Run 2) was conducted to a 6 in. wafer with a $2 \mu m \text{ SiO}_2$ layer placed between the Ta_2O_5 layer and the Si substrate. The $2\mu m$ SiO₂ layer was formed by wet oxidation using a CTR-200 compact thermal reactor furnace. Figure 9 depicts the PCW SEM image after Ta₂O₅ etch, followed by Cr wet etch (to remove the Cr hard mask) and a 5 min dip in 40% KOH at 70 °C. The KOH dip was used to remove microdebris from the $2 \mu m$ trenches as well as from the holes of the PhCs. KOH smooths the surface at the expense of removing a thin layer of SiO₂, since the reaction rate between 40% KOH and SiO₂ is extremely slow at 70 °C, around 200 nm/h.²

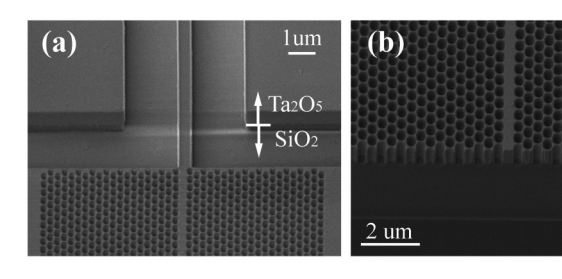


FIG. 9. PCW SEM image with 45 tilt degree after Ta_2O_5 etch, Cr wet etch (to remove the Cr hard mask) and 5 min 40% KOH dip at 70 °C: (a) junction of the PCW and wire waveguide and (b) cross section of PCW.

However, this debris-removing method is not applicable to chips with only a Ta_2O_5 layer above the Si substrate, as KOH reacts rapidly with Si, at a rate of approximately $38\,\mu\text{m/h}$. The chips were tilted 45° when performing SEM imaging, allowing the removed thin SiO_2 layer to be clearly observed in Fig. 9(a). The PhC sidewall maintains a perfect vertical shape in Fig. 9(b), suggesting that the $2\,\mu\text{m}$ SiO_2 layer underneath made little difference to the etching process of Ta_2O_5 .

IV. CONCLUSIONS

This paper focuses on optimizing the ICP etching process to enhance the sidewall profile of the Ta2O5 PCW, characterized by a minimum PhC dimension of pitch 300 nm and diameter 185 nm. A set of experiments was conducted to map the process space and determine the optimal combination of etching parameters, including RF platen power, ICP power, $%C_4F_8$ in gas mixture $(C_4F_8$ and $O_2)$, and chamber pressure. Following this, the best experimental conditions obtained were used as a starting point to investigate the individual impact of each parameter on ICP-RIE. Each parameter was varied once at a time, while keeping the other three constant, to assess their effects on both the etch rate and the sidewall angle. The results are as follows: (1) increasing RF power enhances the physical etching rate but results in angled sidewalls; (2) increasing ICP power accelerates etching rates and provides a better sidewall, but introduces a rougher surface; (3) maintaining a %C₄F₈ in total gas flow of 50% is crucial, as deviations (either too high or too low) lead to undesirable effects, such as increased micromasking or isotropic sidewalls; and (4) higher pressure increases polymer deposition rate, thus, slows the Ta₂O₅ etching rate, accompanied by heightened micromasking. In essence, a delicate balance over the four parameters is essential for etching results. The proposed recipe comprises 50 W RF platen power, 2000 W ICP power, 10 mTorr chamber pressure, and a 50% C₄F₈ in total gas flow (100 SCCM), resulting in an etch rate of 113.325 nm/min and a smooth vertical sidewall in PhCs. Additionally, this configuration is applicable for Ta₂O₅ etching with a $2 \mu m \text{ SiO}_2$ layer underneath, maintaining the integrity of the PhC sidewall.

AUTHOR DECLARATIONS

Conflict of Interest

Ta2O: -SiO2

Si

The authors have no conflicts to disclose.

Author Contributions

Wenjie Wang: Writing – original draft (lead). Libe Arzubiaga: Writing – original draft (supporting). Maryam Shayesteh: Writing – review & editing (equal). Stephen Fenner: Resources (supporting). Owain Clark: Methodology (lead). Martin D. B. Charlton: Project administration (lead).

DATA AVAILABILITY

The data that support the findings of this study are available from the corresponding author upon reasonable request.

REFERENCES

¹C. Chaneliere, J. Autran, R. Devine, and B. Balland, Mater. Sci. Eng. R: Rep. 22, 269 (1998).

M. Belt, M. L. Davenport, J. E. Bowers, and D. J. Blumenthal, Optica 4, 532 (2017).
 R. Fan et al. Sci. Rep. 11, 7978 (2021).

⁴B. S. Ahluwalia, O. G. Hellesø, A. Z. Subramanian, N. M. Perney, N. P. Sessions, and J. S. Wilkinson, Proc. SPIE **7604**, 76040W (2010).

⁵Z. Zhang et al., Opt. Lett. 48, 5799 (2023).

⁶A. Talneau, F. Lemarchand, A. Fehrembach, J. Girard, and A. Sentenac,
Microelectron. Eng. 87, 1360 (2010).

⊆

⁷J. D. Joannopoulos, S. G. Johnson, J. N. Winn, and R. D. Meade, *Photonic Crystals: Molding the Flow of Light*, 2nd ed., revised (Princeton University, Princeton, 2008).
 ⁸M. Butt, S. N. Khonina, and N. Kazanskiy, Opt. Laser Technol. 142, 107265 (2021).

⁹P. S. J. Russell, AIP Conf. Proc. 1176, 3 (2009).

¹⁰N. Rivera and I. Kaminer, Nat. Rev. Phys. 2, 538 (2020).

¹¹M. Soljačić and J. D. Joannopoulos, Nat. Mater. 3, 211 (2004).

¹²D. K.-T. Ng, C. W. Lee, V. Krishnamurthy, and Q. Wang, Adv. Eng. Mater. 20, 1700465 (2018).

¹³M. J. Madou, Fundamentals of Microfabrication and Nanotechnology, Three-Volume Set (CRC, Boca Raton, FL, 2018), https://www.taylorfrancis.com/books/mono/10.1201/9781315274164/fundamentals-microfabrication-nanotechnology-three-volume-set-marc-madou.

¹⁴G. S. May and C. J. Spanos, Fundamentals of Semiconductor Manufacturing and Process Control (John Wiley & Sons, New York, 2006).

15S. Franssila, Introduction to Microfabrication (John Wiley & Sons, New York, 2010).
16K. Lee, K. Jung, R. Singh, S. Pearton, C. Hobbs, and P. Tobin, J. Vac. Sci. Technol. A 18, 1169 (2000).

¹⁷K. Lee, H. Cho, R. Singh, S. Pearton, C. Hobbs, and P. Tobin, J. Vac. Sci. Technol. B 18, 293 (2000).

¹⁸M. F. A. Muttalib, R. Y. Chen, S. J. Pearce, and M. D. Charlton, J. Vac. Sci. Technol. A **32**, 041304 (2014).

¹⁹R. Boucher, W. Morgenroth, H. Roth, H. Meyer, C. Liguda, and M. Eich, J. Vac. Sci. Technol. B 22, 519 (2004).

²⁰H. Sidel, L. Csepregi, A. Heuberger, and H. Baumgärtel, J. Electrochem. Soc. 137, 3626 (1990).